Biomaterials xxx (2012) 1–10

Contents lists available at SciVerse ScienceDirect

Biomaterials

journal homepage: www.elsevier.com/locate/biomaterials

The biocompatibility and antibacterial properties of collagen-stabilized, photochemically prepared silver nanoparticles

Emilio I. Alarcon [a,**,1], Klas Udekwu [b,1], Mårten Skog [c], Natalia L. Pacioni [a], Kevin G. Stamplecoskie [a], María González-Béjar [a], Naresh Polisetti [c], Abeni Wickham [c], Agneta Richter-Dahlfors [b,***], May Griffith [c,d,****], Juan C. Scaiano [a,c,*]

[a] Department of Chemistry and Centre for Catalysis Research and Innovation, University of Ottawa, 10 Marie Curie, Ottawa, ON K1N 6N5, Canada
[b] Swedish Medical Nanoscience Centre, Department of Neuroscience, Karolinska Institute, S-17177 Stockholm, Sweden
[c] Integrative Regenerative Medicine Centre, Linköping University, Department of Clinical and Experimental Medicine, 58185 Linköping, Sweden
[d] University of Ottawa Eye Institute, Ottawa, ON K1H 8L6, Canada

ARTICLE INFO

Article history:
Received 23 January 2012
Accepted 10 March 2012
Available online xxx

Keywords:
Silver nano particles
Type-I collagen
Poly-L-Lysine
Cell toxicity
Antimicrobial activity

ABSTRACT

Spherical 3.5 nm diameter silver nanoparticles (AgNP) stabilized in type I collagen (AgNP@collagen) were prepared in minutes (5–15 min) at room temperature by a photochemical method initiated by UVA irradiation of a water-soluble non-toxic benzoin. This biocomposite was examined to evaluate its biocompatibility and its anti-bacterial properties and showed remarkable properties. Thus, while keratinocytes and fibroblasts were not affected by AgNP@collagen, it was bactericidal against *Bacillus megaterium* and *E. coli* but only bacteriostatic against *S. epidermidis*. In particular, the bactericidal properties displayed by AgNP@collagen were proven to be due to AgNP in AgNP@collagen, rather than to released silver ions, since equimolar concentrations of Ag are about four times less active than AgNP@collagen based on total Ag content. This new biocomposite was stable over a remarkable range of NaCl, phosphate, and 2-(N-morpholino)ethanesulfonic acid concentrations and for over one month at 4 °C. Circular dichroism studies show that the conformation of collagen in AgNP@collagen remains intact. Finally, we have compared the properties of AgNP@collagen with a similar biocomposite prepared using α-poly-L-Lysine and also with citrate stabilized AgNP; neither of these materials showed comparable biocompatibility, stability, or anti-bacterial activity.

1. Introduction

Silver ions or salts and more recently, silver nanoparticles (AgNP) have been used in a wide range of anti-bacterial and anti-fungal applications from clothing and fabrics, washing machines, water purification, toothpaste, fabrics, deodorants, filters, kitchen utensils, toys, and humidifiers to a range of wound dressings [1]. Other proposed nanosilver applications in the biomedical area include: drug delivery [2], molecular imaging of cancer cells [3], coated catheters for cerebrospinal fluids [4,5], inhibition of HIV-1 replication [6,7], anti-inflammatory activity [8], and as a coating for pelvic reconstruction [9]. In regenerative medicine, nanocrystalline silver has been clinically tested to promote healing of chronic leg ulcers [10] as well as to provide bacterial resistance in methacrylate-based bone cements used to secure prostheses in joint replacements [11].

The term silver nanoparticles (AgNP) covers a wide range of nanostructures produced using different methods, leading to various sizes, morphologies and stabilities. The diversity has made any conclusive documentation of the benefits vs. risks challenging [1]. Recent laboratory toxicological studies have suggested that AgNP can be toxic where, for example, clinical studies shown that chronic exposure to silver could have adverse effects on several organs including oral toxicity, liver and kidney damage [12–14]. However, most of these studies have been performed without proper characterization of silver nanomaterial stability and consideration of the preparation method [1,14].

* Corresponding author. Department of Chemistry and Centre for Catalysis Research and Innovation, University of Ottawa, 10 Marie Curie, Ottawa, ON K1N 6N5, Canada. Tel.: +1 613 562 5728; fax: +1 613 562 5170.
** Corresponding author. Tel.: +1 613 562 5728; fax: +1 613 562 5170.
*** Corresponding author.
**** Corresponding author. Integrative Regenerative Medicine Centre, Linköping University, Department of Clinical and Experimental Medicine, 58185 Linköping, Sweden
E-mail addresses: tito@photo.chem.uottawa.ca, titoscaiano@mac.com (J.C. Scaiano).
[1] Equal contributions.

0142-9612/$ – see front matter © 2012 Elsevier Ltd. All rights reserved.
doi:10.1016/j.biomaterials.2012.03.033

Silver nanoparticles can be produced through many methods [14]. These synthetic routes are frequently based on complex protocols involving harsh conditions, making them impractical for large-scale production [11,15–18]. In recent years, the Scaiano group has developed an easy methodology for the synthesis of Au, Cu, and Ag nanoparticles involving ion reduction by ketyl radicals derived from benzoin photoinitiators upon UVA exposure [19–25]. The metal nanomaterials are stable for months or even years, as is the case of Ag and Au nanoparticles, respectively [20,22], and offers excellent control of nanoparticle morphology and size [20,26,27].

Silver nanoparticles have been stabilized by capping with a range of materials including the sacrificial oxidation of Tryptophan-containing peptides [28]. Thus, our aim was to develop AgNP with high biocompatibility while retaining potent anti-microbial properties using a robust biocompatible matrix as protecting agent. To stabilize AgNP using type I collagen, the most abundant protein found in the human body, would be a significant achievement, since we have previously demonstrated the capacity for collagen-based hydrogels to regenerate corneal tissues and nerves in animal models [29] and, most recently, in clinical trials [30]. In cases of bacterial or viral keratitis in the eye or ulcerated skin, an effective anti-microbial or anti-viral, such as AgNP, agent that shows biocompatibility and capacity to induce regeneration would be of great benefit [5–7,11,31]. Here, we report the photochemical synthesis, characterization, *in vitro* biocompatibility and anti-bacterial performance of collagen-coated AgNP as a potential anti-microbial agent. For comparison, we also examined α-poly-lysine and citrate stabilizers, as well as ionic silver. To the best of our knowledge, AgNP-based composite synthesis has not been reported by using either type I collagen or poly-L-Lysine as an integral part of the composite material.

2. Materials and methods

2.1. Chemicals

α-Poly-L-Lysine 0.01% solution (Product numbers P4707, pLL-1, MW range 75–150 kDa and P4832, pLL-2, MW range 150–300 kDa) and $AgNO_3$ were purchased from Sigma–Aldrich. 2-Hydroxy-1-[4-(2-hydroxyethoxy)phenyl]-2-methyl-1-propanone (I-2959) was a generous gift from Ciba Specialty Chemicals. 4-(2-hydroxyethoxy)benzoic acid (4-HEBA) was synthesized according to a reported procedure [32]. Briefly, 13.9 g of 4-hydroxybenzoic acid and 15.0 g KOH were added to 50 mL (1:2.3) H_2O:ethanol. Once dissolved, the mixture was heated under constant stirring to 80 °C and 7.4 mL of 2-chloroethanol in 4.0 mL of ethanol added dropwise in about 2 h. The resultant solution was refluxed overnight with constant stirring. This solution was concentrated by rota-evaporation and the residue was dissolved in 100 mL of water, washed twice with ether and acidified with HCl to obtain a white solid precipitate, which was filtered and dried under vacuum. Finally, the solid was recrystallized from ethanol to obtain white crystals. ^{1}H and ^{13}C-NMR spectra were recorded in a 400 MHz-Brucker; ^{1}H NMR (DMSO-d_6, δ in ppm): 3.74 (m, 2H), 4.06 (t, 2H), 4.87 (broad, 1H), 7.02 (d, 2H, $J = 8.8$ Hz), 7.90 (d, 2H, $J = 8.8$ Hz, 12.65 (broad, 1H); ^{13}C NMR (DMSO-d_6, δ in ppm): 167.5, 162.8, 132.0, 131.8, 123.3, 115.6, 114.6, 70.2, 59.9. Type I medical grade porcine collagen (TheraCol®) was obtained as a 10 ± 1 mg/mL (≈33 μM) acidic aqueous solution and stored at 4 °C until used.

2.2. Synthesis and characterization of AgNP@Collagen and Poly-l-Lysine@AgNP nanocomposites

Aqueous solutions containing 0.2 mM $AgNO_3$, 0.2 mM I-2959 and different concentrations of α-poly-L-lysine (0.4–96 mg/mL) were deoxygenated by purging with N_2 for 30 min followed by exposure to UVA irradiation at 25.0 ± 0.5 °C in a temperature controlled Luzchem CCP-4V photoreactor as previously described [25]. Two different molecular weight ranges of α-poly-L-lysine (pLL) were employed as 70–150 kDa and 150–300 kDa, designated as pLL-1 and pLL-2, respectively. The same irradiation setup was employed to prepare collagen-based nanocomposites. Briefly, aqueous solutions containing 0.2 mM of $AgNO_3$ and I-2959 under N_2 and different aliquots of type I collagen stock solution 10 ± 1 mg/mL (≈33 μM) were added into the reaction media and purged for another 20 min before irradiation. The reaction evolution was monitored at the plasmon absorption band. Spectra were acquired with a 1515 nm/min scan rate at room temperature in a Cary-100-Bio UV–Visible spectrophotometer by using 0.7 cm pathlength cuvettes.

Silver nanoparticles were also characterized by scanning electron microscopy (SEM) in a JSM-7500F FE-SEM from JEOL. Samples for microscopy were prepared by delivering *ca.* 5 μL of solution on carbon-coated copper grids (400 mesh) and allowed to evaporate overnight in a vacuum system prior to imaging. X-ray photoelectron spectroscopy (XPS) was carried out in a Kratos analytical model Axis Ultra DLD, using monochromatic aluminum Kα X-rays at a power of 140 W. Nanoparticle sizes were calculated from SEM imaging by using ImageJ software [33] and in all cases the reported values correspond to the average sizes from at least four different regions in a single grid. Finally, zeta potential (ζ) and hydrodynamic sizes (HS) were measured in a Malvern Zetasizer Nano ZS. HS measurements were carried out at 20 °C using 1.0 cm pathlength disposable cuvettes, while disposable 0.5 mL folded capillary cells (from Malvern) were employed for zeta potential (ζ) measurements.

2.3. Type I collagen and Poly-L-Lysine secondary conformational changes promoted by nanoparticle formation

In order to elucidate possible biopolymer conformational changes accompanying AgNP formation, circular dichroism (CD) measurements were carried out in a Jasco J-810 spectropolarimeter (1.0 nm data pitch, continuous scanning mode, 20 nm/min scan rate). CD measurements (25 ± 0.2 °C) were performed in a 1.0 and 0.1 cm pathlength quartz cells for PLL and collagen, respectively. For collagen denaturation experiments, solution temperature was varied from 20 to 50 °C (1 °C/min) by using a Peltier temperature-controller.

2.4. Biocomposites stability over-time experiments

The stability of our nanocomposites over time was evaluated as follows: 2.0 mL samples were stored at 4.0 °C in darkness in a 0.70 cm optical pathlength quartz cuvettes (Luzchem Inc.) and the absorption spectra measured for up to 39 days for Poly-l-Lysine@AgNP and 68 days for citrate@AgNP and collagen-based AgNP. In addition, 0.1 mL samples were incubated at 37 °C, 5.0% CO_2, 100% humidity and darkness in a 96 well plate for 0.5, 3, 6 and 20 h and their absorbance measured at 405 nm in a SpectraMax 5 plate reader from Molecular Devices. These experiments were performed in different media as follows: (i) in aqueous solution containing different types of AgNP without any additives; (ii) in Dulbecco buffer pH 7.4 in the absence or presence of different calf serum concentrations (from 0.156% to 10%), and, (iii) in keratinocytes serum free medium (KSFM) 5% and 50% v/v.

2.5. Protein peroxides content evaluation

Peroxide formation in type I collagen before and upon UVA irradiation in the presence or absence of $AgNO_3$ and I-2959 was evaluated after 15 min irradiation by using Peroxo-Quant (from Thermo). This method, also called FOX assay, is based on the Fe(II) to Fe(III) oxidation promoted by water-soluble peroxides that produces Xylenol orange/Fe(III) complex, strongly absorbing at 550 nm [34].

2.6. Biocompatibility and cytotoxicity assays

The biocompatibility and cytotoxicity of AgNP and their precursors was evaluated *in vitro* on two human primary cell lines, dermal fibroblast and epidermal keratinocytes (ATCC, USA) at low passage number (between 1 and 5). The fibroblasts were grown in Dulbecco's modified eagle's medium (DMEM, Gibco) containing 10% fetal calf serum and penicillin/streptomycin (Lonza Walkersville), and cultured at 37 °C, 5.0% CO_2 in a humidified incubator. The keratinocytes were cultured in keratinocytes serum free medium containing L-Glutamine (KSFM, Gibco). Biocompatibility was evaluated by using CellTiter 96® Aqueous MTS (3-(4,5-dimethyl-2-tiazol)-2,5-diphenil-2H-tetrazolium bromide; tiazol blue) colorimetric viability assay (Promega) [35] and employed as a measure of cell survival after 14 h of incubation. Briefly, from confluent cell cultured, 5×10^4 cell/mL (cell counting was carried out in a Scepter 2.0 handheld automated cell counting from Millipore®) were seeded in a 96-well plate followed by incubation for 6 h, prior to addition of nanoparticles or precursors at various dilutions. The samples were incubated for 14 h after which the well contents were replaced by fresh medium (100 μL), and 20 μL of MTS solution added followed by incubation at 37 °C, 5.0% CO_2 and 100% humidity for 2 and 4 h for fibroblasts and keratinocytes, respectively. The absorbance was then recorded at 490 nm in a Victor well plate reader, at 20 °C.

Dead-live measurements: Viability/Cytoxicity Kit for mammalian cells (Invitrogen L-3244, Carlsbad, CA). Human fibroblasts were seeded as described previously for MTS assay and after 14 h of incubation the cells were washed out with PBS and incubated in 4 μM ethidium, 2 μM calcein solution for 30 min. Fluorescent images were captured with a Zeiss LSM 700 confocal microscope.

2.7. Antimicrobial activity

We evaluated the anti-microbial activity of the AgNP prepared here, against the gram (+) bacteria *Bacillus megaterium* (Strain *Bm11*) and *Staphylococcu epidermis* (Strain *Se4*) as well as the uropathogenic strain of the gram (−) bacterium *Escherichia coli* (CFT073).

Please cite this article in press as: Alarcon EI, et al., The biocompatibility and antibacterial properties of collagen-stabilized, photochemically prepared silver nanoparticles, Biomaterials (2012), doi:10.1016/j.biomaterials.2012.03.033

*Minimal inhibitory concentration (MIC):*The MIC of each compound:bacteria combination was determined by broth microdilution method, slightly modified from the standard Clinical and Laboratory Standards Institute (CLSI) protocol [36], in cation-adjusted Muller Hinton II (CAMHII) and Luria Bertani broth (LB). Briefly, an overnight culture from a single colony was diluted to a cell density of ~5×10^5 colony forming units (*cfu*) per mL in either broth containing two-fold dilutions of the test compounds. The absorbance was estimated at 600 nm (OD_{600}) measured at time 0 and after 18 h of incubation at 37 °C. The lowest concentration of test-substance at which the absorbance of the bacterial inoculum did not increase substantially ($\Delta OD_{600} < 0.03$ OD units/18 h) was taken as the MIC. The MIC was determined as that concentration at which no net increase in absorbance was observed and designated as MIC_{LB} or MIC_{CMH} for LB-estimated and CAMHII-estimated values. All measurements were carried out by triplicate in two independents days and median results reported.

Time kill assay (TK): Exponentially growing cultures of the three test bacteria were exposed for 3 h in 6-well plates (FALCON™), to 1x and 2x MIC_{LB} concentrations of each test-substance while constantly stirred at 37 °C. Intermittently, over 3 h, survivor population density was estimated by plating saline-diluted samples on LB agar and allowing for growth at 37 °C for 24–48 h. The enumeration of survivors was by manual count or using a BioRad gel documentation system combined with the colony counting module of the commercial Quantity One™ software. All results are expressed as the mean of three to five replicates per timepoint ± SE (standard error) and each experiment was repeated at least once on a different day with essentially the same results.

Growth inhibition of AgNP@collagen biocomposites: *E.coli*, *S.epidermidis* and *B.megaterium* overnight cultures were diluted 250x in LB and allowed to acclimatize at 37 °C fro 1 h prior to inoculating into 96-well plates containing two-fold dilutions (in LB) of each test compound. The inoculum size was approximately 5×10^5 cfu/mL in assay volumes of 100 µl per well. Growth was monitored at 37 °C in a Biotek™ scanner by measuring the absorbance (OD_{600}) of each well while the plate was vigorously agitated over 18 h. Each experiment was carried out at least two more times on different days and by duplicate on each test 96 well plate. Each curve represents an average of two replicates from one such representative assay.

*Solid anti-bacterial activity (SAA):*The anti-bacterial activity of AgNP was also explored by using halo formation in agarose gel containing 1.0×10^7 cfu/mL. Briefly, 3.0 mm diameter holes were punched into a 1% agarose gel containing the bacterium at approximately the above cell density and 5.0 µL of AgNP solutions at different concentrations added, followed by overnight incubation at 37 °C. Where observed, inhibitory halos (if observed) were measured and the anti-bacterial performance estimated from the diameter of the zone of inhibition compared to what is observed with streptomycin.

3. Results and discussion

3.1. Photochemical synthesis of silver nanoparticles

Several metallic ions, *i.e.* Au^{+3}, Cu^{+2} and Ag^{+}, can be efficiently reduced upon UV radiation in the presence of benzoin compounds such as Irgacure-2959 [22–25]. Specifically, AgNP have been synthesized in aqueous and organic media by this procedure (see Scheme 1) [21,25], usually in the presence of stabilizing agents such as citrate to prevent particle aggregation or oxidation. In fact, aqueous citrate stabilized AgNP (*vide infra*) exhibit a negative zeta potential of ≈ −40 mV, consistent with their stability.

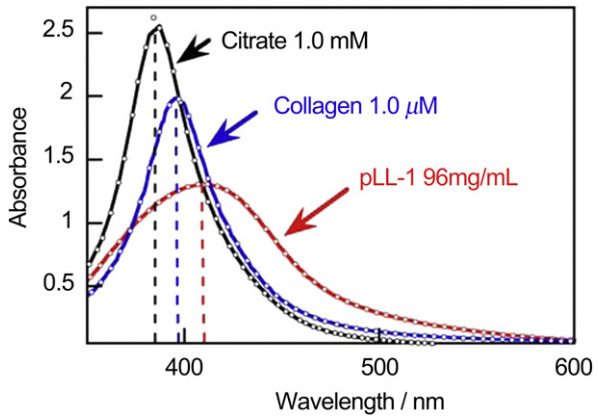

Fig. 1. Absorption spectra for colloidal AgNP prepared by using different stabilizers; 1.0 mM sodium citrate (black line), 1.0 µM type I collagen (blue line), and 96 mg/mL pLL-1 (red line) upon 1.03 mW/cm^2 UVA irradiation for 5 min. Vertical dashed lines included in the plot indicate maximum absorption wavelength for each AgNP. All measurements were carried out at room temperature in N_2 saturated solutions. (For interpretation of the references to color in this figure legend, the reader is referred to the web version of this article.)

3.2. Photochemical synthesis of biomolecule-stabilized silver nanoparticles

Once Ag^0 has formed, nucleation forms Ag clusters and eventually colloidal AgNP. As mentioned before, AgNP need a protecting agent, otherwise particle oxidation or aggregation occurs readily. Sodium citrate is a common stabilizing agent, however, an important shortcoming for medical applications is its anticoagulant activity, more powerful than heparin [37]. Thus, we decided to replace this protecting agent for a more biocompatible one such that it would possess: (i) Water solubility (up to mM); (ii) Biocompatibility (low toxicity or biodegradable), and (iii) Transparent in the 315–400 nm range (UVA).

Several UVA transparent L-aminoacids, such as Lys, His, Met, and Cys were tested; however, only marginal or no AgNP protection was afforded (in the best case L-Lys; AgNP were stable for <30 min, data not shown). This lack of stability is probably due to poor interactions between the metallic surface and the aminoacid. Thus, we tested two common biopolymers, structures that can improve the protection of the metallic surface, such as type I collagen (Col-I) and α-poly-L-Lysine (pLL). Both polymers are transparent to UVA light and do not have any oxidable aminoacidic residues, *i.e.*, Trp, Tyr, or Phe [28]. After UVA exposure of samples containing either Col-I or pLL in the presence of I-2959 and Ag^+, stable AgNP (*vide infra*) with

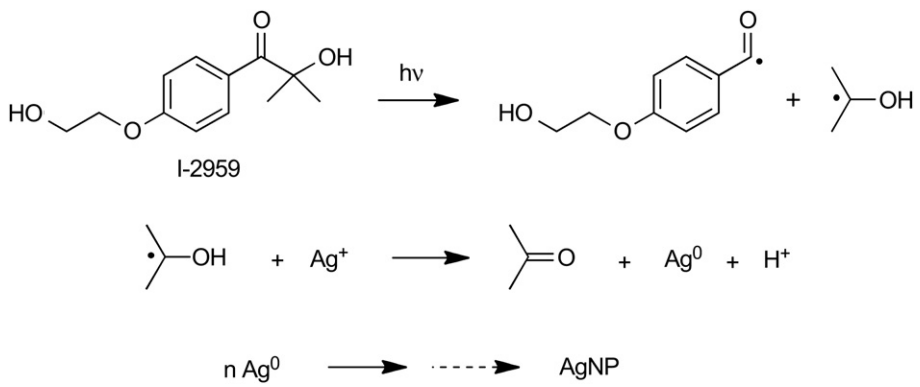

Scheme 1. Photoreduction of Ag^+ by ketyl radicals produced by I-2959 UVA excitation. Stabilizing agent has been omitted from this scheme (see text).

Please cite this article in press as: Alarcon EI, et al., The biocompatibility and antibacterial properties of collagen-stabilized, photochemically prepared silver nanoparticles, Biomaterials (2012), doi:10.1016/j.biomaterials.2012.03.033

a surface plasmon band (SPB) ~390–410 nm were observed (see Fig. 1). The SPB maximum for AgNP prepared in the presence of pLL is slightly red shifted to 408 nm when compared with citrate stabilized AgNP (λ_{max} 397 nm) [25]. Similar results have been observed for other AgNP prepared using biomacromolecular stabilizers [17]; further, when Col-I is employed, the SPB is at ≈390 nm, probably due to the presence of relatively small particles. We have not noted any evidence for nanoparticle morphology changes for Col-I or pLL, since the additional absorption bands, that are expected for other AgNP shapes, were absent [25]. Both materials showed a single Ag oxidation state (most likely Ag^0) as revealed from XPS measurements with peaks centered at binding energies of 366.0 eV and 367.7 eV for Col-I and pLL, respectively (see Fig. S1). The optimal UVA dose to make the smallest pLL-protected AgNP, ≈10 nm diameter, was determined as 1.03 mW/cm^2 (see SI for details; Figs. S2–S4 and Table S1); we employed that dose to prepare AgNP using Col-I.

Collagen forms more than 30% of the human body, and type I collagen is the most abundant in connective tissue and skin [38]. Fig. 2 shows the SPB increase as a function of irradiation time by using 1.03 mW/cm^2 UVA dose in the presence of 1.0 μM collagen. Importantly, the initial slope of the integrated SPB, between 350 and 600 nm, shows an inverse dependence with the protein concentration becoming smaller with increasing protein concentration (inset Fig. 2). Additionally, the decrease in the I-2959 absorption band at 280 nm that stops after 7.5 min irradiation (see Fig. 2) indicates complete initiator photodecomposition compatible with total silver reduction (confirmed by XPS). Similar results were observed for pLL (see Figs. S5 and S6). Remarkably, the SPB intensities when using 96 mg/mL pLL-1 decrease to approximately 60% compared with citrate stabilized AgNP (Fig. 1 and page S8), something not observed when Col-I is the protecting agent.

In addition, scanning electron microscopy measurements carried out for AgNP prepared by using 0.5 μM Col-I (AgNP@collagen) reveal the presence of spherical AgNP (≈3.5 nm), Fig. S7. However, when the protein concentration is increased the image quality deteriorated due to the excess of organic material that burns easily under our conditions (data not shown). Despite this, the presence of AgNP plasmon absorption in all cases shown in Figs. 1 and 2 is conclusive evidence for AgNP formation in the presence of Col-I at all the protein concentrations used.

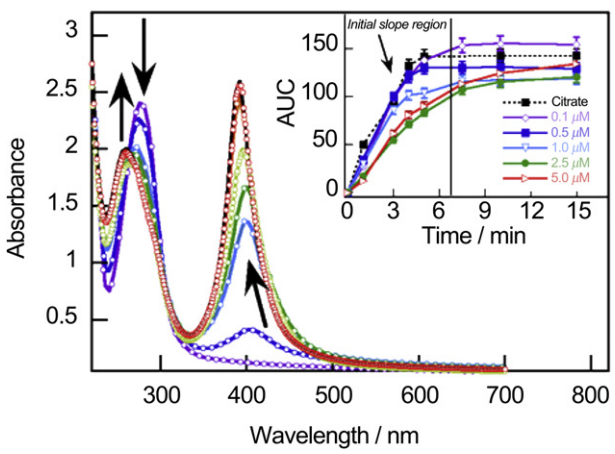

Fig. 2. Absorption spectra for colloidal AgNP prepared by using 1.0 μM type I collagen as stabilizing agent upon 1.03 mW/cm^2 UVA irradiation for up to 15 min (see arrow). Inset: Dependence of the area under the curve (*see text*) obtained at different protein concentrations from 0.1 to 5.0 μM; in this plot the initial slope region is denoted by an arrow (*area under the curve for citrate@AgNP time profile has been also included for comparison*). All measurements were carried out at room temperature in N_2 saturated solutions; error bars of 15% have been included in the plot.

The photochemical preparation of metal nanoparticles leads to the generation of substituted benzoyl radicals, which in the presence of traces of oxygen produce peroxyl radicals that could attack the protein promoting oxidation. For this reason, we decided to measure peroxide content in the protein prior and after AgNP formation in the presence of Col-I (see Fig. S8). No detectable peroxides were observed (see page S11 for more details). Nevertheless, this does not guarantee the absence of conformational changes in the protein secondary structure after AgNP formation as documented for other systems [39–41]. Thus, UV-CD measurements of the protein secondary conformation in the presence of AgNP were carried out.

Fig. S9A shows that in collagen UV-CD spectra neither position (195.5 and 220 nm) nor intensity (see inset Fig. S9A), are affected by the presence of AgNP, which suggests collagen's conformation is preserved. Indeed, no changes were observed for the Rpn parameter (an indicator of triple helix conservation in collagen expressed as 220 and 195.5 nm ratio), even 16 days after AgNP preparation (see Fig. S9B), for all the protein concentrations, except for the 0.1 μM sample. Thus, our findings indicate that AgNP does not modify the right handed triple helix of type I collagen [42] in contrast to pLL (Fig. S10). Furthermore, zeta potential (ζ) values smaller than ≈ ±20 mV are insufficient to generate the required Coulombic repulsion and promotes nanoparticle aggregation [43]. Interestingly, the negatively charged nature of our citrate@AgNP (−40 mV) turns into a positively stable particles (Col-I > 0.5 μM and pLL > 30 mg mL^{-1}) indicating that both polypeptides protect the surface of AgNP (Figs. S11 and S12). This effect is notably enhanced in pLL nanocomposites reaching values close to +70 mV (see Fig. S12) probably due to the multiple pLL chains on the surface.

We also found that all Col-I capped nanocomposite formulations were stable under a wide range of NaCl concentrations (Fig. S13A) while only at pLL > 60 mg mL^{-1} stabilized pLL@AgNP (Fig. S13B) as compared with citrate@AgNP (aggregated > 30 mM NaCl, Fig. S13A). Similar results were observed for AgNP in phosphate (pH 7.4, Fig. S13C) and MES buffer (pH 5.0, Fig. S13D); where only Col-I nanocomposites showed a remarkable stability. Differences in nomenclature (pLL@AgNP vs. AgNP@collagen) reflect observed differences in protection and the fact that in Col-I AgNP are believed to be fully encapsulated by the protein structure.

3.3. *Stability of AgNP@collagen and PLL@AgNP role of biomacromolecular conformation on the nanoparticle stability*

Silver nanoparticles prepared by using pLL-1, pLL-2, and collagen concentration between 0.5 and 2.5 μM are stable in aqueous solutions for over 30 days (see SI page S17 and Fig. S14 for more details). Thus, collagen-based AgNP synthetized outside the stability range (*i.e.*, with 0.1 or 5.0 μM collagen) will be excluded in the following sections. Colloidal AgNP solutions exist only in the presence of a dispersant media. However, if there is an efficient stabilizing agent surrounding the nanoparticle, plasmonic absorbance is anticipated even when the solvent has been removed. In our case, Fig. S15 shows representative pictures of polystyrene weighting boats where 5.0 μL drops of aqueous solutions containing collagen-based AgNP, pLL-1@AgNP, pLL-2@AgNP, and citrate@AgNP were delivered and evaporated for 12 h at 8 °C.

The results shown in Fig. S15 for particles prepared in the presence of Col-I support incorporation of AgNP within the protein, and agree with the higher stability of the nanocomposite in NaCl, phosphate buffer and MES aqueous solutions (Fig. S13). Thus, we use AgNP@collagen to label the collagen-based

Please cite this article in press as: Alarcon EI, et al., The biocompatibility and antibacterial properties of collagen-stabilized, photochemically prepared silver nanoparticles, Biomaterials (2012), doi:10.1016/j.biomaterials.2012.03.033

nanocomposites prepared. Moreover, variation in the media temperature will affect the protein conformation differently depending on the type of macromolecule employed. For example, in very structured proteins such as Col-I, which conformation is controlled mainly by the coexistence of triple Gly-X-Y chains, a temperature increase will cause intrachain disruption and irreversible denaturation [38]. In contrast, for biopolymers poorly structured, as poly-L-Lysine, a temperature decrease will produce a more organized structure.

Fig. 3 shows the effect of temperature decrease at 1.0 °C/min for AgNP@collagen (1.0 μM), pLL-1@AgNP, and citrate@AgNP. This figure shows that sample freezing affects differently AgNP SPB for each system. In the first case SPB appears to be still present (Fig. 3A and C), but the presence of new additional yellow "sticks" surrounding the solid in the center of the tube was observed (showed more clearly in TOC), probably due to a more organized structure formed by AgNP decorating the biomacromolecule in the solid state. Nevertheless, after total sample thawing there was only a minor effect on the SPB of the nanoparticle (Fig. 3C) as well as in the protein conformation (data not shown). Interestingly, for pLL-1@AgNP the original yellow color turns reddish suggesting sample aggregation (Fig. 3D and E). In fact, Fig. 3F shows the pLL-1@AgNP absorption spectra for the sample before and after freezing indicating particle aggregation due to the new red shifted absorption at ≈600 nm. In fact, AgNP HS size increases from 15 nm to 140 nm (similar trends were observed for pLL-2, data not shown). Surprisingly, citrate@AgNP SPB is apparently bleached after freezing (Fig. 3G), and gradually recovers when thawing starts (see Fig. 3H), attributable to a change in the medium refractive index during-water solidification with a minimal effect on the SPB (see Fig. 3I).

In order to evaluate how a temperature increase can affect nanoparticle stability, absorption spectra for citrate@AgNP, pLL-1@AgNP and AgNP@collagen were measured over a temperature range (within 20 and 50 °C, 1.0 °C/min), Fig. S16. Interestingly, only for AgNP@collagen, a temperature increase above 45 °C modifies both shape and intensity of plasmonic absorption in an irreversible way (see SI8 for more details). Thus, CD measurements for collagen alone or in the nanocomposite were also carried out in the 20–50 °C range employing 1.0 °C/min rate (Fig. S17A and B for collagen alone or in the presence of AgNP, respectively). Two distinct regions on Rpn values were observed when increasing the temperature. The first one, between 20 and 39 °C, where almost no changes are observed, and, a second region, from 39 to 50 °C

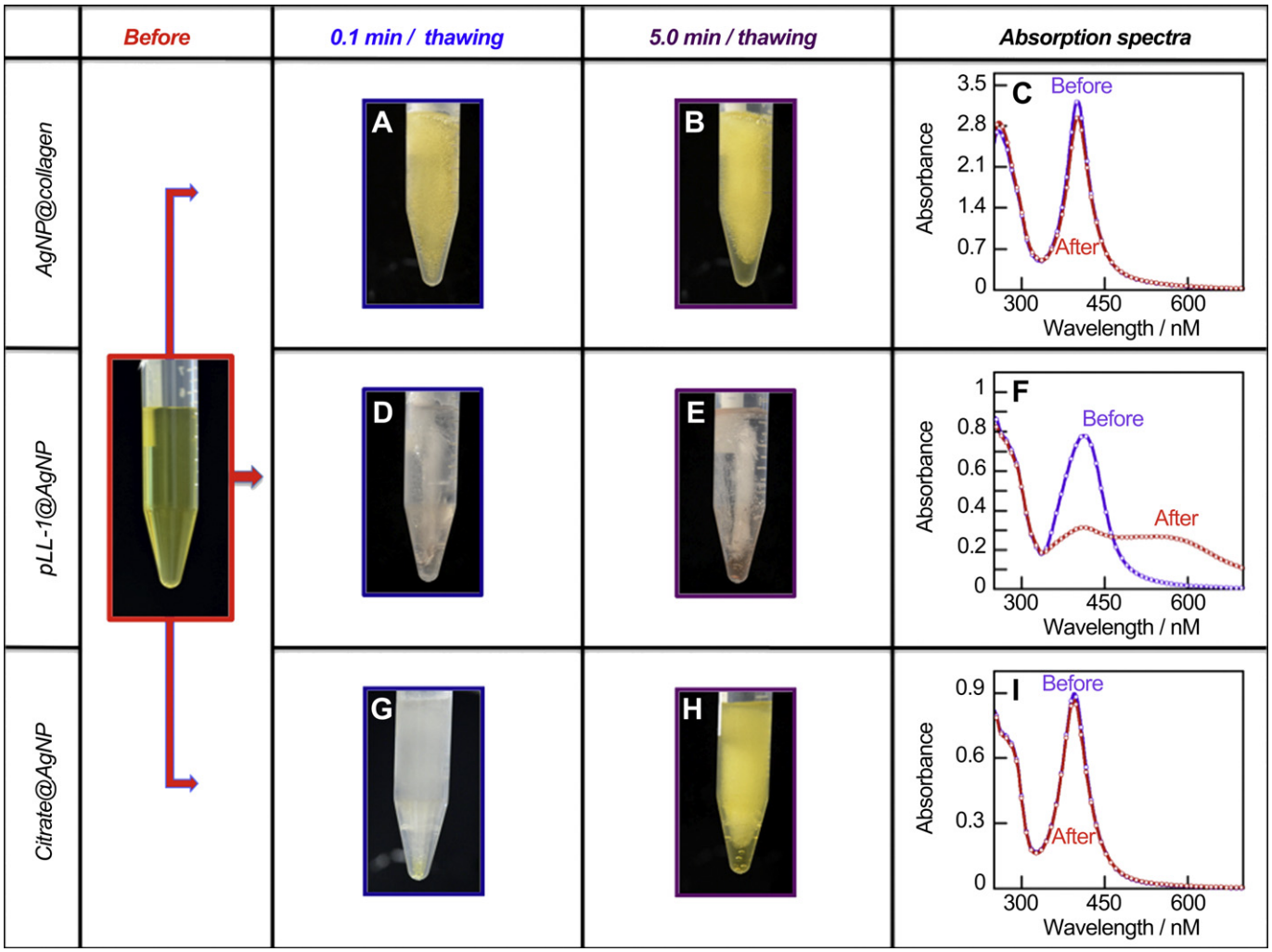

Fig. 3. Effect of sample freezing (rate = −1.0 °C/min) on AgNP plasmonic absorbance for AgNP@collagen 1.0 μM (A–C), pLL-1@AgNP (D–F), and citrate@AgNP (G–I). Pictures were taken at room temperature at different times (0.1 and 5.0 min) after start of thawing using a Nikon D7000 using a Lens: Sigma 105 mm F2.8 EX DG Macro. In order to prevent water condensation on the tube a gentle N_2 flow was employed in all cases.

Please cite this article in press as: Alarcon EI, et al., The biocompatibility and antibacterial properties of collagen-stabilized, photochemically prepared silver nanoparticles, Biomaterials (2012), doi:10.1016/j.biomaterials.2012.03.033

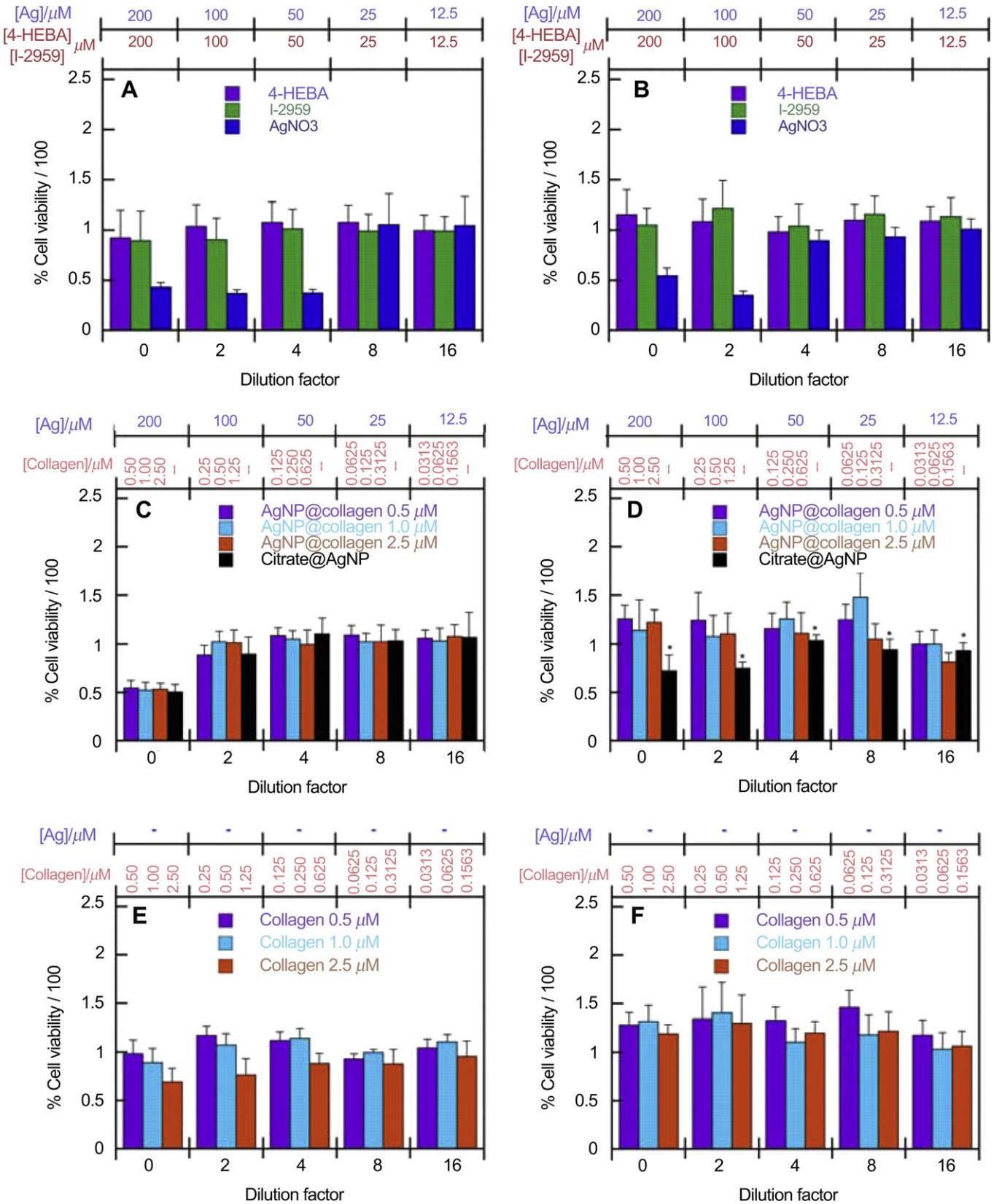

Fig. 4. Cell viability measurements carried out by using MTS® colorimetric assay (see experimental section) of human fibroblasts (left column) and human keratinocytes (right column) after 14 h incubation (A, B) in the presence of different concentrations of 4-HEBA, I-2959, and $AgNO_3$; (C, D) AgNP@collagen prepared by using 0.5, 1.0, and 2.5 μM collagen or citrate@AgNP; and finally (F, E) type I collagen cytotoxicity at different concentrations (0.5, 1.0, and 2.5 μM). Silver concentration has been expressed as the total in each experiment, independently particle aggregation/size (top blue). Error bars correspond to the average of three independent measurements (triplicate experiments) calculated by using error propagation methodology in all cases $p > 0.10$ from one-way ANOVA analysis carried out in KaleidaGraph® version 4.2. Asterisks in Figure D indicate particle spontaneous aggregation in KSFM. (For interpretation of the references to color in this figure legend, the reader is referred to the web version of this article.)

Please cite this article in press as: Alarcon EI, et al., The biocompatibility and antibacterial properties of collagen-stabilized, photochemically prepared silver nanoparticles, Biomaterials (2012), doi:10.1016/j.biomaterials.2012.03.033

denaturation region, where this value decreases with a slope ≈0.018 and 0.020 Rpn units/°C for collagen alone and in the presence of AgNP, respectively. From the intersection point of both regions we obtained a value close to 40 °C for protein denaturation with or without AgNP, which agrees with the value for dermal bovine type I collagen [42].

In summary, AgNP@collagen present excellent stability over a range of different conditions that could facilitate their biomedical applications, *i.e.* human skin scaffold where type I collagen has been employed in hydrogel scaffold [29]. Specifically, the potential anti-bacterial properties of AgNP [4,5,11,14,31] should be of interest for the treatment of chronic leg ulcers [10]. With these applications in mind, we examined the cytotoxicity in human fibroblasts and keratinocytes as well as the anti-bacterial activity against *Staphylocous Epidermis, Bacilus Megaterium and Eschericha Coli* of AgNP@collagen and compared with the activity of pLL-1@AgNP, pLL-2@AgNP, and citrate@AgNP.

3.4. Biocompatibility and cytotoxicity of AgNP@collagen, pLL@AgNP and citrate@AgNP

Incubation of various NP samples in cell-free media showed that 10% FSC in DMEM prevented the aggregation of pLL-1@AgNP and citrate@AgNP (see Fig. S18), while AgNP@collagen showed no serum-dependent response, consistent with the incorporation of AgNP into the collagen structure. Further, in KSFM, either citrate or pLL-protected AgNP spontaneously aggregate (see Fig. S19A and B) and only Col-I nanocomposites were stable (Fig. S19C). Thus, in order to evaluate the biocompatibility and potential cytotoxicity of our materials, their toxicity in human fibroblasts (varying FCS concentration, or keeping it constant at 10% no significant differences were observed, only data obtained using 10% FCS has been included here) and keratinocytes (grown in free FCS media) was evaluated using the MTS assay [35] (*Note:* Similar results were obtained for human fibroblasts if the incubation keeping 10% FCS was carried out using PBS or DMEM; data not shown). Non-toxicity for I-2959 (photoinitiator) or 4-HEBA (photoproduct) was established in all cell-cultured lines employed here (see Fig. 4A–B). Although, $AgNO_3$ was toxic at dilution factors lower than 4 and 2 for fibroblasts and keratinocytes, respectively. Additionally, pLL-1 and pLL-2 (Fig. S20A and B) appear to be equipotent cytotoxic than their respective pLL@AgNP at dilutions lower than 8 (see Fig S20C and D).

Human keratinocytes were affected by these compounds as depicted in Fig. 4F. In addition, mostly independently of the cell-line employed here, low toxicity was detected at dilutions higher than 2.0 when AgNP@collagen (Fig. 4C and D) or type I collagen alone as shown in Fig. 4E and F. Citrate@AgNP seems to be more toxic for human keratinocytes (Fig. 4D). However, no direct comparison between the toxicity observed in keratinocytes and fibroblasts, by Citrate@AgNP, can be obtained since these particles spontaneously aggregate in keratinocytes culture medium (Fig. 4D). More interestingly, $AgNO_3$ toxicity only resembles to Citrate@AgNP if they are aggregated as shown in Fig. 4C and D.

There is an important point related with the toxicity of AgNP and their stability as well as the understanding of cell nanoparticle interaction, specifically when comparing two different nanomaterials. Thus, in addition to the completely different nature of both cell lines (metabolism, cell membrane, and morphology) the aggregation state and stability of the biomaterial needs to be considered *i.e.* only for AgNP@collagen no aggregation was observed in either fibroblasts (PBS or DMEM) and keratinocytes media (see Figs. S18 and S19), but when citrate@AgNP was employed total aggregation of the nanoparticle takes place in the absence of FCS. Similar survival fibroblasts population was obtained from live-dead fluorescence protocol as displayed in Fig. S21 (see Page S22 for more details).

3.5. Antimicrobial properties

Three bacterial species were chosen in order to assess the antibacterial activity of AgNP composites. They are representative of sporulating and non-sporulating gram (+) bacteria (*B.megaterium and S.epidermidis*, *respectively*) as well as the pathogenic gram (−) enteric bacterial strain of *E.coli, CFT073*. Testing for growth inhibition by the broth-microdilution MIC assay, we observed that for each bacterium, μM concentrations of total silver were at least as growth inhibitory as $AgNO_3$ controls. This was the case for both pLL-, (not shown) and AgNP@collagen nanoparticles although in the former, the conjugate molecule alone was as anti-microbial as the conjugated one, but notably only collagen-based composites do not aggregate (see Table 1 for MIC values). Table 1, shows the role of test medium and concentration on MIC values. In almost all cases, the estimated MIC was higher in the cation-adjusted MHII medium. Notably, the AgNP in their conjugated form were at least as effective as $AgNO_3$ at inhibiting the growth of the bacteria tested. These data were corroborated in our growth inhibition assays carried out in 96-well plates and summarized in Fig. 5. This Figure shows that the collagen-based silver nanocomposite (at 1.0 μM in collagen) has an improved activity with increasing lag time for bacterium growth at much lower concentrations than those employed for either citrate@AgNP or ionic silver as $AgNO_3$; similar trends were observed for the other two AgNP@collagen formulations (data not shown) confirming that collagen is more than a simpler stabilizing agent for these nanocomposites.

MICs and growth inhibition experiments alone cannot differentiate between bactericidal and bacteriostatic activity, otherwise discernible under time-kill conditions [44,45]. Further, there is a profound density related effect on the efficacy of most antibiotics for at the very least staphylococci [46]. Thus, short-term (3 h) time-killing studies were performed for each of the collagen-conjugated

Table 1
Estimated MICs (in μM Ag content) in Lysogeny broth (LB) and cation-adjusted Muller Hinton broth (MHII). Assay was carried out according to CLSI broth microdilution protocol [36].

	LB			MHII		
	E. coli	*B. megaterium*	*S. epidermidis*	*E. coli*	*B. megaterium*	*S. epidermidis*
AgNP@collagen 0.5 μM	25	3.13	12.5	50	12.5	25
AgNP@collagen 1.0 μM	25	3.13	12.5	50	6.25	12.5
AgNP@collagen 2.5 μM	12.5	1.56	6.25	25	12.5	12.5
$AgNO_3$	25	6.25	12.5	12.5	6.25	12.5
Citrate@AgNP	50	6.25	12.5	50	6.25	25
pLL-1@AgNP	12.5	1.56	3.13	12.5	6.25	12.5
pLL-2@AgNP	25	1.56	3.13	25	12.5	12.5
pLL-1	100	3.13	6.25	50	6.25	12.5
pLL-2	50	3.13	3.13	50	6.25	12.5

Please cite this article in press as: Alarcon EI, et al., The biocompatibility and antibacterial properties of collagen-stabilized, photochemically prepared silver nanoparticles, Biomaterials (2012), doi:10.1016/j.biomaterials.2012.03.033

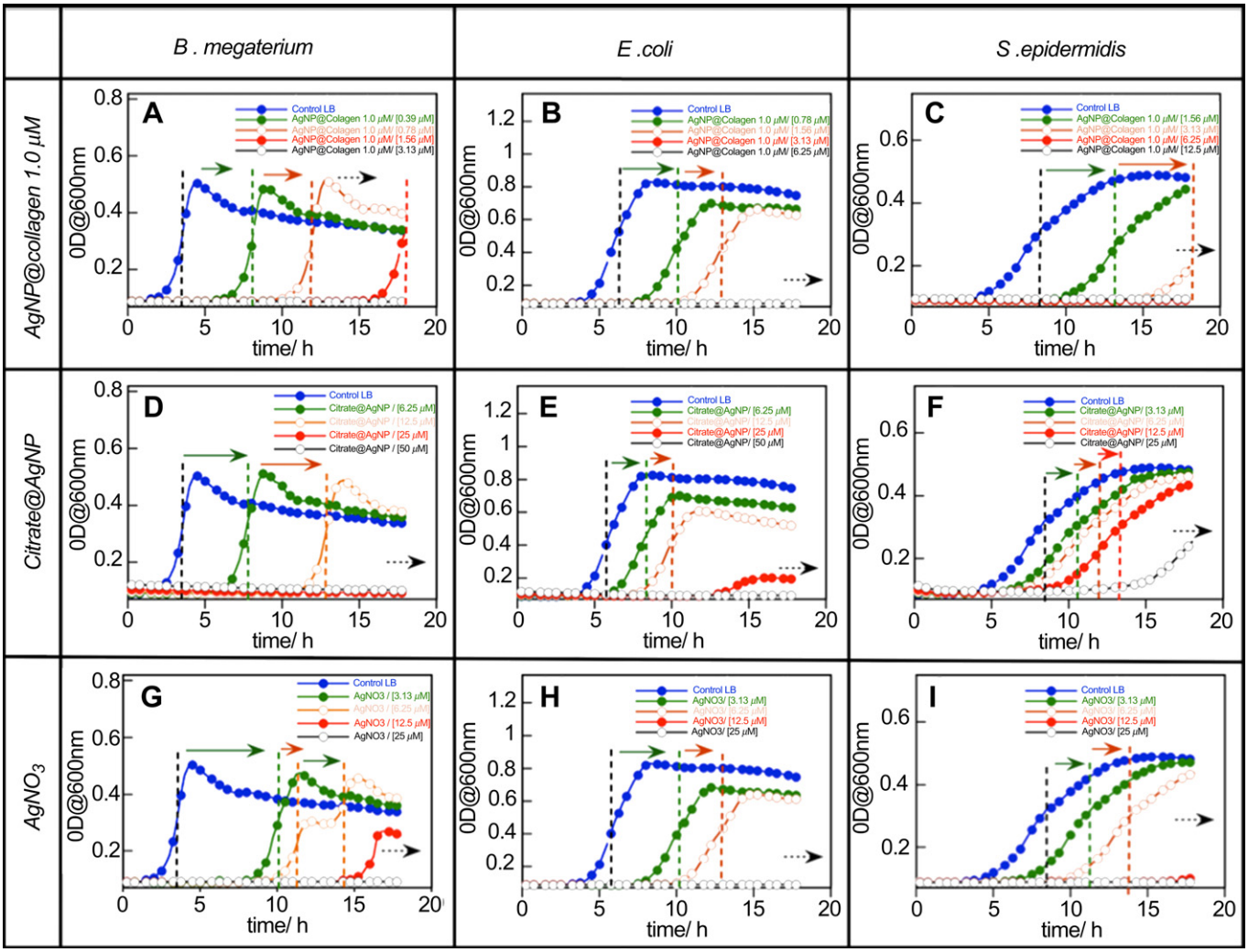

Fig. 5. Bacteria growth inhibition profile for *B. megaterium (left column), E.coli (middle column), and S.epidermidis (right column)* up to 18 h in the presence of different concentrations, as indicated in each figure, of (A–C), AgNP@collagen 1.0 μM, (D–E), citrate@AgNP (F-H), and $AgNO_3$ (M–O). Dashed colored lines indicate the time where a 50% of the maximal OD at the plateau level is reached. Thus, as a result product of the addition of compounds into LB medium there was an increase in this time that is indicated by the horizontal arrows inserted there. An additional black dashed horizontal arrow is also included that indicates that longer lag times are expected for all the other concentrations that did not show up at times shorter than 18 h.

nanoparticles and for pLL-1@AgNP. Each species was challenged at low density ($\sim 5 \times 10^5$ cfu ml^{-1}), with 1x and 2x MIC concentrations of each of the materials. These results are shown in Fig. 6 for *B. megaterium,* and in *E. coli, and S. epidermidis* respectively. For *B. megaterium* and *E. coli*, there is a net decline in cell density as a result of exposure to 1x and 2x MIC concentrations for 1.0 μM collagen-conjugated NP see Fig. 6A and B, similar results were obtained for the other formulations (data not shown). For $AgNO_3$ only for *E.coli* a net decline in the bacteria population was observed (see Fig. 6H). In the case of *S.epidermidis* however, no significant decline is observed in cell density during the course of the assay and the AgNP as well as $AgNO_3$ are effectively bacteriostatic (Fig. 6 right column).

Based on the kinetics of killing, *B.megaterium* is more susceptible to the 1.0 μM (Fig. 6A) and 2.5 μM collagen-conjugated AgNP than to equivalent concentrations of the positive control. Importantly, this contrasts with the growth inhibition results where 0.5 and 1.0 μM concentrations inhibited growth better than 2.5 μM AgNP@collagen at equivalent concentrations. The reason for this is as yet unclear although differential killing efficacy has been observed in several cases of quinolone and fluoroquinolone antibiotics [46,47]. However, as reduced sensitivity is noted for the 0.5 μM collagen-conjugated NP (not shown) in the time-killing assay, collagen is implicated in either stabilization of, or otherwise increasing the efficacy of the nanoparticles.

This view is enhanced by the observation that citrate@AgNP (these particles aggregated spontaneously in the cell culture medium) are consistently more similar to the $AgNO_3$ (Fig. 6D–G) controls than the conjugated nanoparticles. Consistent with the noted differential efficacies of antibiotics, a different scenario is observed for *E.coli*: Firstly, collagen nanocomposites are all notably more bactericidal at this concentration (Fig. 6B) than citrate@AgNP (which are aggregated); particles that are only slightly bactericidal at 1x MIC (Fig. 6E) while ionic silver as $AgNO_3$ is highly toxic at these concentrations (see Fig. 6H). Differences between the two conjugated nanoparticles are not discernible as the bacterial culture is rapidly cleared at 1x and 2x MIC. No significant difference is noted between the observed killing profiles for all collagen nanocomposites within the time frame of the assay, 3 h (Fig. 6). Lastly, *S.epidermidis* susceptibility was primarily bacteriostatic at the concentrations tested (right column Fig. 6). This was the case when we looked at higher AgNP concentrations (data not shown).

Please cite this article in press as: Alarcon EI, et al., The biocompatibility and antibacterial properties of collagen-stabilized, photochemically prepared silver nanoparticles, Biomaterials (2012), doi:10.1016/j.biomaterials.2012.03.033

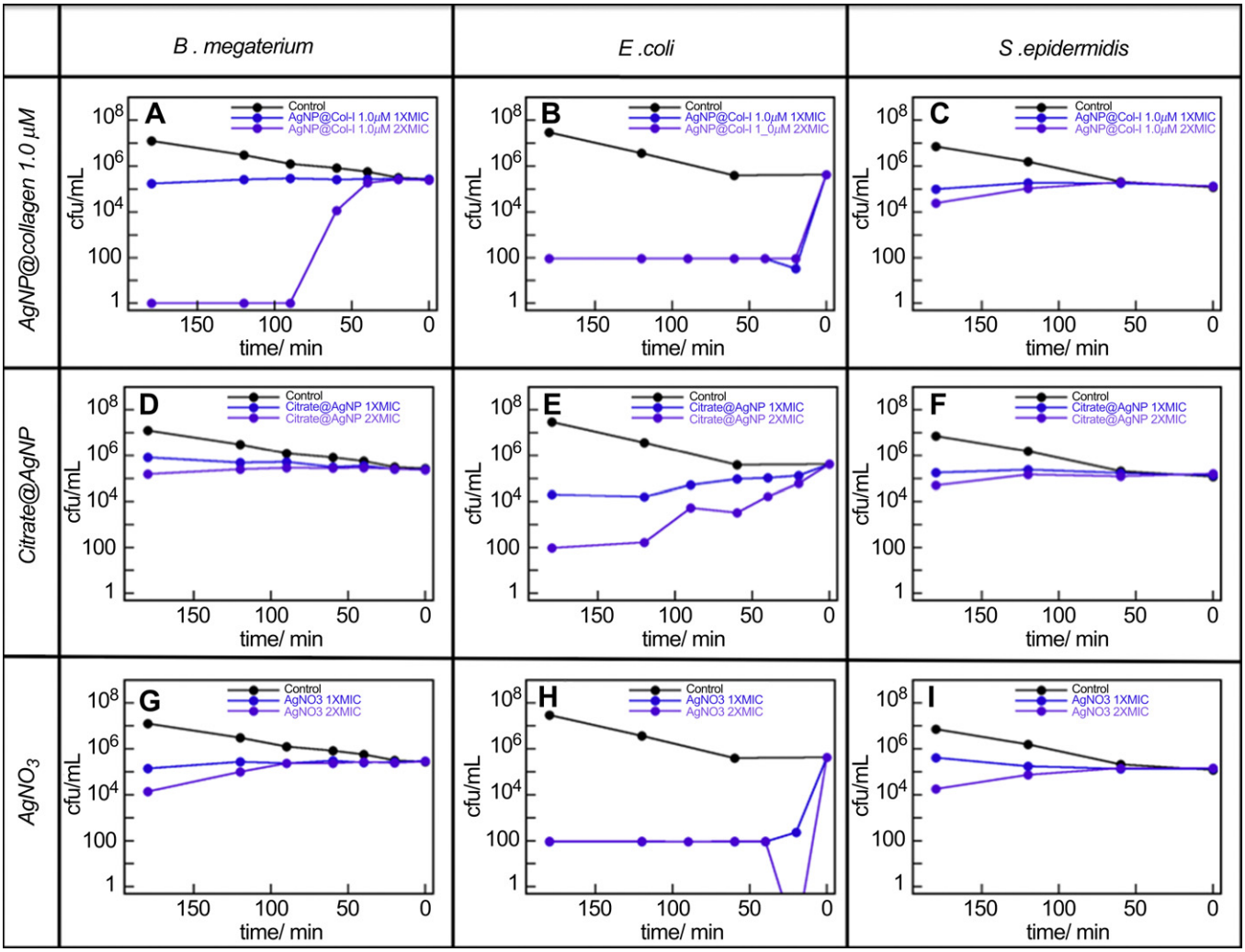

Fig. 6. Bacteria time-kill profiles for *B. megaterium (left column), E.coli (middle column), and S.epidermidis (right column)* up to 180 min in the presence of AgNP@collagen 1.0 μM (A–C), citrate@AgNP (D–F), and $AgNO_3$ (G–I) at either 1xMIC or 2xMIC (see Table 1). Data reported here correspond to the average of three independent measurements (by quadruplicate each experiment), error was lower than 10% of the mean in all cases.

Insignificant differences were observed between the activity of the AgNP, Ag^+ and even pLL-conjugated AgNP. Note that for all bacteria, the pLL-conjugated NP and pLL controls were equivalently inhibitory to growth implying that the bactericidal efficacy of such conjugated NP was mostly dependent on the conjugant (Table 1 and data not shown). Additionally, in order to explore AgNP activity in semisolid state, we assessed their efficacy on bacterial populations embedded in 1% agarose as previously described in the testing of anti-microbial peptides [48]. These studies were inconclusive as no apparent inhibition zones were observed in any of the test cases, whether Ag^+ or conjugated/unconjugated AgNP were used.

Thus, our anti-microbial cumulative data point to the efficacy of AgNP is strongly affected by conjugation as showed for silver nanoparticles conjugated to type I collagen, where the macromolecule may be the source of improved efficacy compared to the 'seed' AgNP.

4. Conclusions

In summary, we report the synthesis, characterization, *in-vitro* biocompatibility, and anti-bacterial activity against *B. megaterium*, *E. coli,* and the highly clinically relevant *staphylococcu epidermis* bacteria of a new type I collagen "coated" AgNP nanocomposite material prepared using a photochemical approach in 5–15 min at room temperature. Comparison with the results obtained with poly-L-Lysine as capping agent. We showed that biomacromolecular conformation impacts on AgNP stability; poly-L-Lysine capped nanoparticles suffer from spontaneous aggregation at higher ionic strength or lower temperature. In contrast, AgNP prepared with type I collagen, displayed extraordinary stability. More importantly, these collagen-based nanocomposites seem to be stable in cell culture media showing non-toxic effects even at dilutions 2x against both human fibroblasts and keratinocytes. Moreover, we have found that the presence of fetal calf serum in the cell-cultured media prevents the formation of aggregates of citrate capped AgNP and less efficiently of AgNP conjugated with poly-lysine (pLL). Finally, collagen-stabilized AgNP were bactericidal against *B. megaterium* and *E.coli* but only bacteriostatic against *S.epidermidis*, however this was not longer observed in solid phase assays. Our findings concerning the action of AgNP suggest that the bacterial mode of killing by AgNP can be influenced by the stability of the particle itself.

Acknowledgments

The Natural Sciences and Engineering Research Council (NSERC, Canada) supported this work through its Discovery and CREATE programs. KU and ARD thanks to the Swedish Research Council, contract no. 621-2010-5189. EA thanks to Becas Chile for a post-doctoral contract. We would also like to express our special

thanks to Michel Grenier for his help on sample's photography and to Mrs Madleen Zapata for designing several Figures. JCS acknowledges his appointment as visiting professor at Linköping University.

Appendix A. Supplementary material

Supplementary material associated with this article can be found, in the online version, at doi:10.1016/j.biomaterials.2012.03.033.

References

[1] Varner KE, El-Badawy A, Feldhake D, Venkatapathy R. State-of-the-science review: everything nanosilver and more. Washington, DC, US: U.S. Environmental Protection Agency; 2010.
[2] Skirtach AG, Oz JA, Kreft O, Hler K, Piera Alberola A, Hwald H, et al. Laser-induced release of encapsulated materials inside living cells. Angew Chem Int Ed Engl 2006;45(28):4612–7.
[3] Tai SP, Wu Y, Shieh BD, Chen LJ, Lin KJ, Yu CH, et al. Molecular imaging of cancer cells using plasmonresonant-enhanced third-harmonic-generation in silver nanoparticles. Adv Mater 2007;19(24):4520–3.
[4] Bayston R, Ashraf W, Fisher L. Prevention of infection in neurosurgery: role of 'antimicrobial' catheters. J Hosp Infect 2007;65(Suppl. 2):39–42.
[5] Galiano K, Pleifer C, Engelhardt K, Brossner G, Lackner P, Huck C, et al. Silver segregation and bacterial growth of intraventricular catheters impregnated with silver nanoparticles in cerebrospinal fluid drainages. Neurol Res 2007; 30(3):285–7.
[6] Elechiguerra JL, Burt JL, Morones JR, Camacho-Bragado A, Gao X, Lara HH, et al. Interaction of silver nanoparticles with HIV-1. J Nanobiotechnol 2005;29(3):6.
[7] Sun RW, Chen R, Chung NP, Ho CM, Lin CL, Che CM. Silver nanoparticles fabricated in HEPES buffer exhibit cytoprotective activities toward HIV-1 infected cells. Chem Commun 2005;28(40):5059–61.
[8] Shin SH, Ye MK, Kim HS, Kang HS. The effects of nanosilver on the proliferation and cytokine expression by peripheral blood mononuclear cells. Int Immunopharmacol 2007;7(13):1813–8.
[9] Cohen MS, Stern JM, Vanni AJ, Kelley RS, Baumgart E, Field D, et al. In vitro analysis of a nanocrystalline silver-coated surgical mesh. Surg Infect (Larchmt) 2007;8(3):397–403.
[10] Sibbald RG, Contreras-Ruiz J, Coutts P, Fierheller M, Rothman A, Woo K. Bacteriology, inflammation, and healing: a study of nanocrystalline silver dressings in chronic venous leg ulcers. Adv Skin Wound Care 2007;20(10): 549–58.
[11] Alt V, Bechert T, Steinrücke P, Wagener M, Seidel P, Dingeldein E, et al. An in vitro assessment of the antibacterial properties and cytotoxicity of nanoparticulate silver bone cement. Biomaterials 2004;25(18):4383–91.
[12] Kim YS, Song MY, Park JD, Song KS, Ryu HR, Chung YH, et al. Subchronic oral toxicity of silver nanoparticles. Part Flbre Toxicol 2007;7:20.
[13] Hagens WI, Oomen AG, de Jong WH, Cassee FR, Sips AJ. What do we (need to) know about the kinetic properties of nanoparticles in the body? Regul Toxicol Pharmacol 2007;49(3):217–29.
[14] Sharma VK, Yngard RA, Lin Y. Silver nanoparticles: green synthesis and their antimicrobial activities. Adv Coll Inter Sci 2009;145(1–2):83–96.
[15] Kasthuri J, Veerapandian S, Rajendiranb N. Biological synthesis of silver and gold nanoparticles using apiin as reducing agent. Colloids Surf B Biointerfaces 2009;68(1):55–60.
[16] Eby DM, Schaeublin NM, Farrington KE, Hussain SM, Johnson GR. Lysozyme catalyzes the formation of antimicrobial silver nanoparticles. ACS Nano 2009; 3(4):984–94.
[17] Murawala P, Phadnis SM, Bhonde RR, Prasad BLV. In situ synthesis of water dispersible bovine serum albumin capped gold and silver nanoparticles and their cytocompatibility studies. Colloids Surf B Biointerfaces 2009;73(2): 224–8.
[18] Wu Q, Cao H, Luan Q, Zhang J, Wang Z, Warner JH, et al. Biomolecule-assisted synthesis of water-soluble silver nanoparticles and their biomedical applications. Inor Chem 2008;47(13):5882–8.
[19] McGilvray KL, Decan MR, Wang D, Scaiano JC. Facile photochemical synthesis of unprotected aqueous gold nanoparticles. J Am Chem Soc 2006;128(50): 15980–1.
[20] Marin ML, McGilvray KL, Scaiano JC. Photochemical strategies for the synthesis of gold nanoparticles from Au(III) and Au(I) using photoinduced free radical generation. J Am Chem Soc 2008;130(49):16572–84.
[21] Maretti L, Billone PS, Liu Y, Scaiano JC. Facile photochemical synthesis and characterization of highly fluorescent silver nanoparticles. J Am Chem Soc 2009;131(39):13972–80.
[22] Scaiano JC, Billone P, Gonzalez CM, Maretti L, Marin ML, McGilvray KL, et al. Photochemical routes to silver and gold nanoparticles. Pure Appl Chem 2009; 81(4):635–47.
[23] Gonzalez CM, Liu Y, Scaiano JC. Photochemical strategies for the facile synthesis of gold-silver alloy and core-shell bimetallic nanoparticles. J Phys Chem C 2009;113(27):11861–7.
[24] Pacioni NL, Pardoe A, McGilvray KL, Chretien MN, Scaiano JC. Synthesis of copper nanoparticles Mediated by Photogenerated free radicals: catalytic role of chloride anions. Photochem Photobiol Sci 2010;9(6):766–74.
[25] Stamplecoskie KG, Scaiano JC. Light Emitting Diode irradiation can control the morphology and optical properties of silver nanoparticles. J Am Chem Soc 2010;132(6):1825–7.
[26] McGilvray KL. Photochemical strategies for the synthesis of gold nanoparticles. Ottawa, Canada: University of Ottawa; 2010.
[27] Scaiano JC, Netto-Ferreira JC, Alarcon E, Billone P, Bueno Alejo CJ, Crites C-OL, et al. Tuning plasmon transitions and their applications in organic photochemistry. Pure Appl Chem 2011;83(4):913–30.
[28] Si S, Mandal TK. Tryptophan-based peptides to synthesize gold and silver nanoparticles: a mechanistic and kinetic study. Chemistry 2007;13(11): 3160–8.
[29] Liu W, Deng C, McLaughlin CR, Fagerholm P, Lagali NS, Heyne B, et al. Collagen–phosphorylcholine interpenetrating network hydrogels as corneal substitutes. Biomaterials 2009;30(8):1551–9.
[30] Fagerholm P, Lagali NS, Merrett K, Jackson WB, Munger R, Liu Y, et al. A biosynthetic alternative to human donor tissue for inducing corneal regeneration: 24-month follow-up of a phase 1 clinical study. Sci Trans Med 2010;2(46):46ra61.
[31] Jeon HJ, Yi SC, Oh SG. Preparation and antibacterial effects of Ag–SiO2 thin films by sol–gel method. Biomaterials 2003;24(27):4921–8.
[32] Meng X, Natansohn A, Barret C, Rochon P. Azo polymers for reversible optical storage. 10. Cooperative motion of polar side groups in amorphous polymers. Macromolecules 1996;29(3):946–52.
[33] Rasband WS. ImageJ, U. S. Bethesda, Maryland, USA: National Institutes of Health; 1997.
[34] Jiang Y, Hunt JV, Wolff SP. Ferrous oxidation in the presence of xylenol orange for detection of lipid hydroperoxides in low density lipoproteins. Anal Biochem 1992;202(2):384–9.
[35] Promega Corporation. CellTiter 96® AQueous one solution cell proliferation assay [cited; Available from: http://www.promega.com/resources/protocols/technical-bulletins/0/celltiter-96-aqueous-one-solution-cell-proliferation-assay-system-protocol/; 2009.
[36] Wikler MA. Performance standards for antimicrobial susceptibility testing: fifteenth informational supplement. Wayne, PA. USA: Clinical and Laboratory Standards Institute; 2005.
[37] Monchi M, Berghmans D, Ledoux D, Canivet JL, Dubois B, Damas P. Citrate vs. heparin for anticoagulation in continuous venovenous hemofiltration: a prospective randomized study. Intensive Care Med 2004;30(2):260–5.
[38] Avery NC, Bailey AJ, Barocas VH, Biewener AA, Blank RD, Boskey AL, et al. Collagen: structure and mechanics. LLC 1 ed. New York, US: Springer Science + Business Media; May 30, 2008.
[39] Wu X, Narsimhan G. Effect of surface concentration on secondary and tertiary conformational changes of lysozyme adsorbed on silica nanoparticles. Biochim Biophys Acta A 2008;1784(11):1694–701.
[40] De Paoli Lacerda SH, Park JJ, Meuse C, Pristinski D, Becker ML, Karim A, et al. Interaction of gold nanoparticles with common human blood proteins. ACS Nano 2010;4(1):365–71.
[41] Yang Q, Liang J, Han H. Probing the interaction of magnetic iron oxide nanoparticles with bovine serum albumin by spectroscopic techniques. J Phys Chem B 2009;113(30):10454–8.
[42] Freudenberg U, Behrens SH, Welzel PB, Müller M, Grimmer M, Salchert K, et al. Electrostatic interactions modulate the conformation of collagen I. Biophys J 2007;92(6):2108–19.
[43] Delgado AV, González-Caballero F, Hunter RJ, Koopal LK, Lyklema J. Measurement and interpretation of electrokinetic phenomena (IUPAC technical report). Pure Appl Chem 2005;77(10):1753–805.
[44] Levin BR, Udekwu KI. Population dynamics of antibiotic treatment: a mathematical model and hypotheses for time-kill and continuous-culture experiments. Antimicrob Agents Chemother 2010 Aug;54(8):3414–26.
[45] Regoes RR, Wiuff C, Zappala RM, Garner KN, Baquero F, Levin BR. Pharmacodynamic functions: a multiparameter approach to the design of antibiotic treatment regimens. Antimicrob Agents Chemother 2004;48(10):3670–6.
[46] Udekwu KI, Parrish N, Ankomah P, Baquero F, Levin BR. Functional relationship between bacterial cell density and the efficacy of antibiotics. J Antimicrob Chemother 2009;63(4):745–57.
[47] Crumplin GC, Smith JT. Nalidixic acid: an antibacterial paradox. Antimicrob Agents Chemother 1975;8(3):251–61.
[48] Putsep K, Branden CI, Boman HG, Normark S. Antibacterial peptide from *H. pylori*. Nature 1999;398(6729):671–2.